ELSEVIER

www.elsevier.nl/locate/jorganchem

Journal of Organometallic Chemistry 614–615 (2000) 243–254

Journal of Organometallic Chemistry

Synthesis, characterization, structural and theoretical analysis of a series of electron deficient, monomeric thallium iron carbonylate isostructural and isolobal to diiron nonacarbonyl

Kenton H. Whitmire [a,*], Ilse Y. Guzman-Jimenez [a], Jean-Yves Saillard [b], Samia Kahlal [b]

[a] *Department of Chemistry, Rice University, PO Box 1892, Houston, TX 77251, USA*
[b] *Laboratoire de Chimie du Solide et Inorganique Moléculaire, UMR CNRS 6511, Université de Rennes 1, 35042 Rennes Cedex, France*

Received 5 May 2000

Dedicated to Professor Sheldon Shore on the occasion of his 70th birthday.

Abstract

Extended Hückel and density functional calculations on the isoelectronic $[Fe_2(CO)_6(\mu\text{-}CO)_{3-n}\{\mu\text{-}TlFe(CO)_4\}_n]^{n-}$ $(n = 0–3)$ series show that the nature of the Fe···Fe interaction is quite similar within the series, despite of the different observed internuclear separations. An orbital explanation is provided to explain why these compounds are diamagnetic despite of the absence of a real Fe–Fe bond. In the cases of $n = 1–3$, the formation of dimers allows the release of the electron deficiency on Tl centers through donation from an iron lone pair, leaving almost unchanged bonding within the associated monomers. The stability of the dimers with respect to dissociation appears to be limited by the destabilizing ionic interaction between the negatively charged monomers.

Keywords: Negatively charged monomer; Diagmagnetic; Iron lone pair; Inter nuclear separation

1. Introduction

The structure of diiron nonacarbonyl has been known since its determination by X-ray diffraction in 1939 [1]. The formula is written as $Fe_2(CO)_6(\mu\text{-}CO)_3$ to emphasize its structural features. There has been considerable interest in this molecule arising from the understanding of the nature of the Fe–Fe bonding interaction [2–8]. Ambiguity arises from the presence of the three doubly bridging CO ligands which obscure the interpretation of the metal–metal interaction. It is now generally accepted that there is little direct interaction between the iron atoms as shown by molecular orbital calculations and symmetry arguments [3–8].

Our interest in this discussion revolves around our discovery of a series of thallium-containing iron carbonyl cluster compounds which are isoelectronic to $Fe_2(CO)_6(\mu\text{-}CO)_3$ [9–11]. The parent anion $[Tl\{Fe(CO)_4\}_2]^-$ [12] is readily accessed cleanly and in high yield by reaction of thallium salts with $Fe(CO)_5$ in methanolic KOH and can be isolated as a variety of salts [12]. As the Et_4N^+ salt, it exists as a weak dimer in the solid state ($[Et_4N]_2[\{Tl(Fe(CO)_4)_2\}_2]$, $[Et_4N]_2[\{\mathbf{I}\}_2]$). This dimerization is thought to arise in an attempt to alleviate the electron deficiency at the Tl center.

* Corresponding author. Fax: +1-713-3485515.
E-mail address: whitmir@ruf.rice.edu (K.H. Whitmire).

0022-328X/00/$ - see front matter
PII: S0022-328X(00)00629-X

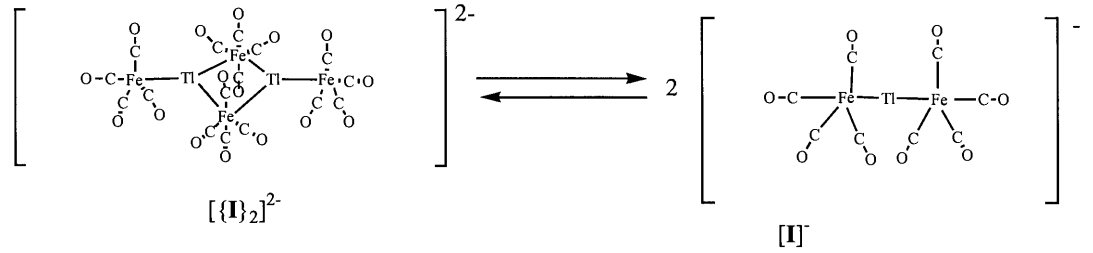

$[\{\mathbf{I}\}_2]^{2-}$ $[\mathbf{I}]^-$ (1)

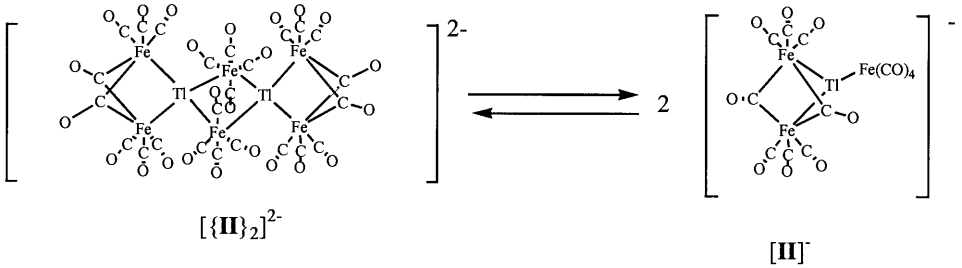

$[\{\mathbf{II}\}_2]^{2-}$ $[\mathbf{II}]^-$ (2)

Metal frameworks containing similar Tl_2Fe_2 core structures have been observed for $[PPN]_2[Tl_2Fe_6(CO)_{24}]$ ($[PPN]_2[\{\mathbf{II}\}_2]$), $[Et_4N]_4[Tl_4Fe_8(CO)_{30}]$ ($[Et_4N]_2[\{\mathbf{III}\}_2]$), and $[Et_4N]_6[Tl_6Fe_{10}(CO)_{36}]$ ($[Et_4N]_2[\{\mathbf{IV}\}_2]$). These anions may also be written as $[\{Fe_2(CO)_6(\mu\text{-}CO)_2(\mu\text{-}Tl(Fe(CO)_4)\}_2]^{2-}$, $[\{Fe_2(CO)_6(\mu\text{-}CO)(\mu\text{-}Tl(Fe(CO)_4)_2\}_2]^{4-}$ and $[\{Fe_2(CO)_6(\mu\text{-}Tl(Fe(CO)_4)_2\}_3]^{6-}$ to emphasize their structural relationship to $Fe_2(CO)_6(\mu\text{-}CO)_3$. These compounds may be thought of as dimeric clusters formed through bonding of electron-rich iron centers of one monomeric unit to electron-deficient thallium atoms of another. The structures show non-bonding Tl···Tl distances ranging from 3.604(3) to 3.859(2) Å. Before the characterization of this series of thallium–iron carbonyl clusters, the only Tl–Fe compound which had been reported was $Tl_2Fe_3(CO)_{12}$ synthesized by W. Hieber; but that compound was formulated solely on the basis of elemental analysis [13].

Using ^{205}Tl-NMR spectroscopy we were able to show that the observed coupling patterns are consistent with the existence of the monomeric forms for $[\mathbf{I}]^-$ and $[\mathbf{III}]^{2-}$ while $[\{\mathbf{II}\}_2]^{2-}$ appeared to remain as the dimer in solution. Thallium-NMR is convenient for this purpose owing to the presence of two naturally-occurring spin 1/2 nuclei — ^{205}Tl and ^{203}Tl — in a 70.5:29.5 ratio. The presence of isotopomers may give rise to coupling patterns between nuclei of the two different isotopes when more than one Tl atom is present in a molecule or ion.

When dissolved in solution, $[\{\mathbf{I}\}_2]^{2-}$ shows only a singlet ^{205}Tl signal (no Tl–Tl coupling) and a simple solution IR spectrum similar to trigonal bipyramidal $Fe(CO)_4L$ compounds as expected for the dissociation into $[\mathbf{I}]^-$. In contrast, the solid-state infrared spectrum shows a more complicated pattern as expected for the lower symmetry. For compound $[\{\mathbf{II}\}_2]^{2-}$, ^{205}Tl–^{203}Tl coupling was observed, giving a triplet ^{205}Tl signal

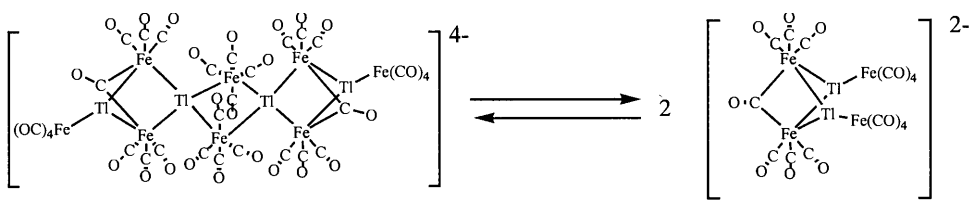

$[\{\mathbf{III}\}_2]^{4-}$ $[\mathbf{III}]^{2-}$

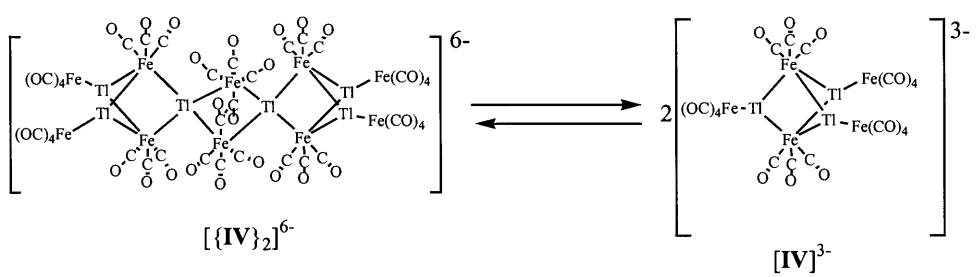

$[\{\mathbf{IV}\}_2]^{6-}$ $[\mathbf{IV}]^{3-}$

consistent with retention of the dimeric structure upon dissolution. The coupling pattern observed is consistent with a structure containing two Tl nuclei arising from the combination of the singlet due to the $^{205}Tl/^{205}Tl$-containing species superimposed upon a doublet from the $^{205}Tl/^{203}Tl$ isotopomer. This compound was thought the least likely to dissociate on the basis of the bond parameters for the central Tl_2Fe_2 ring.

Compound $[\{\mathbf{III}\}_2]^{4-}$ can be viewed as a dimer of two $[Fe_2(CO)_6(\mu\text{-}CO)\{\mu\text{-}TlFe(CO)_4\}_2]^{2-}$ units. If this dimer form for compound $[\{\mathbf{III}\}_2]^{4-}$ were retained in solution, a very complicated coupling pattern would be expected owing to the presence of four thallium atoms giving rise to nine unique $^{205}Tl/^{203}Tl$ isotopomers. Instead a pattern similar to that observed for $[\{\mathbf{II}\}_2]^{2-}$ is observed indicating that only two Tl nuclei are present in the ion and supporting view that the compound dissociates into the monomeric forms in solution.

The loss in electron density at thallium when in the monomer forms may be lessened through solvent donation, although no solvent-coordinated compound has yet been isolated. Compound $[\{\mathbf{I}\}_2]^{2-}$, however, has been observed to react with chelating nitrogen bases to give $[\{(CO)_4Fe\}_2TlL]^-$ complexes (L = bipyridine, phenanthroline, tetramethylethylenediamine, diethylenetriamine, and ethylenediamine) [14].

In this paper we report the structural characterization of a cluster with the formula $[PPN]_3[Fe_2(CO)_6\{\mu\text{-}TlFe(CO)_4\}_3]$ which is the monomer form of the previously reported $[Et_4N]_6[\{\mathbf{IV}\}_2]$. The PPN^+ (bis-(triphenylphosphine)iminium, $Ph_3P{=}N{=}PPh_3^+$) salt of the title compound was synthesized from the reaction of $TlCl_3$ with $Fe_3(CO)_{12}$ in methanolic KOH and shows a markedly different solid state structure from the $[Et_4N]^+$ salt. Having the structural parameters available for the monomer has allowed us to examine in more detail the bonding changes in the family of compounds $[Fe_2(CO)_6(\mu\text{-}CO)_{3-n}\{\mu\text{-}TlFe(CO)_4\}_n]^{n-}$ ($n = 0$–3) as a function of n by the means of extended Hückel theory (EHT) and density functional theory calculations (DFT). We will explore two fundamental aspects of the bonding of this class of compounds: (**1**) the issue of Fe–Fe and Tl–Tl bonding along with the effects on the bonding that replacing the bridging carbonyls of $Fe_2(CO)_6(\mu\text{-}CO)_3$ with the heavy main group element fragments has and; (**2**) the structural and energetic effects of dimerization.

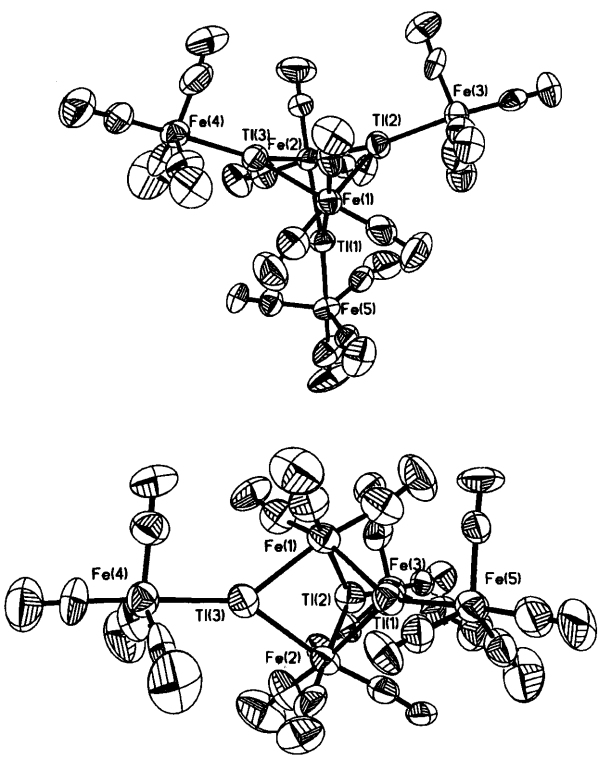

Fig. 1. Thermal displacement ellipsoid plots of two different views of of the anion $[\mathbf{IV}]^{3-}$.

2. Experimental

All manipulations were performed using standard techniques on a Schlenk line or in a Vacuum Atmospheres drybox [15]. The organic solvents used were distilled under argon from the appropriate drying agents [16]. [PPN]Cl was prepared by the literature method [17]. The following materials were used as received from their commercial sources: $Fe_3(CO)_{12}$ (Strem Chemicals), $Tl(OOCCH_3)_3$ (Acros) and KOH (Fischer Scientific).

2.1. Synthesis of [PPN]$_3$[IV]

To a solution of $Fe_3(CO)_{12}$ (1.523 g, 3 mmol) in 50 ml of methanol was added an excess of KOH (1.3 g, 23 mmol). The solution changed color from green to cherry-red characteristic of the $[HFe_3(CO)_{11}]^-$ anion. Solid thallium (III) acetate was added all at once (0.589 g, 1.5 mmol) and the solution changed color from cherry-red to deep brown immediately. The [PPN]Cl (0.908 g, 1.5 mmol) was added as a solid. After stirring for 2 h the reaction mixture was filtered over Celite® 521 through a glass frit. Excess diethyl ether was added to the filtrate and the flask was placed in a refrigerator until crystallization occurred.

2.2. X-ray crystallography

A suitable crystal was encapsulated in a capillary tube and mounted on the tip of a glass fiber with epoxy cement. Data were collected with a Bruker AXS automated CCD diffractometer using the Bruker AXS package and using Mo-K_α radiation ($\lambda = 0.71069$ Å). The structure was solved by direct methods. All non-hydrogen atoms were refined with anisotropic displace-

Table 1
Crystal data and structure refinement for $[PPN]_3$[**IV**]

Empirical formula	$C_{126}H_{90}Fe_5N_3O_{18}P_6Tl_3$
Formula weight	3012.19
Temperature (K)	293(2)
Wavelength (Å)	0.71073
Crystal system	Monoclinic
Space group	$P2_1/c$
Unit cell dimensions	
a (Å)	17.120(3)
b (Å)	50.706(10)
c (Å)	16.785(3)
α (°)	90
β (°)	116.90(3)
γ (°)	90
V (Å^3)	12994(5)
Z	4
D_{calc} (Mg m^{-3})	1.540
Absorption coefficient (mm^{-1})	4.382
$F(000)$	5896
Crystal size (mm)	$0.5 \times 0.2 \times 0.15$
θ Range for data collection (°)	1.33–23.36
Limiting indices	$-18 \le h \le 16$, $-56 \le k \le 56$, $-18 \le l \le 18$
Reflections collected	59466
Independent reflections	18735 ($R_{int} = 0.1749$)
Absorption correction	None
Refinement method	Full-matrix least-squares on F^2
Data/restraints/parameters	18735/0/1204
Goodness-of-fit on F^2	0.823
Final R indices [$I > 2\theta(I)$]	$R_1 = 0.0631$, $wR_2 = 0.1590$
R indices (all data)	$R_1 = 0.2164$, $wR_2 = 0.1969$
Largest difference peak and hole (e Å^{-3})	2.012 and −0.546

ment parameters, and hydrogen atoms were calculated in ideal positions (riding model). Refinement of F^2 was performed using all reflections. The weighted R-factor wR and goodness-of-fit S are based on F^2, conventional R-factors R are based on F, with F set to zero for negative F^2. R-factors based on F^2 are statistically about twice as large as those based on F, and R-factors based on all data will be even larger. All software used is contained in the SHELXTL-5.10 [18] program library. An ORTEP diagram is shown in Fig. 1. Crystal data and structure refinements are listed in Table 1 and selected bond distances and angles are given in Table 2.

3. Computational details

Extended Hückel theory (EHT) and density functional theory (DFT) calculations were performed on a series of $[Fe_2(CO)_6(\mu\text{-}CO)_{3-n}(\mu\text{-}TlR)_n]^{n-}$ [$n = 0$–3; R = H$^+$, Fe(CO)$_4$] monomers, as well as on the dimers $[\{\mathbf{II}\}_2]^{2-}$, $[\{\mathbf{III}\}_2]^{4-}$ and $[\{\mathbf{IV}\}_2]^{6-}$. EHT calculations [19] were carried out with the help of the CACAO package, [20] assuming idealized geometry's based on the averaged experimental structures. The Slater exponents (ζ) and the valence shell ionization potentials (H_{ii} in eV) were respectively: 1.3, −13.6 for H 1s; 1.625, −21.4 for C 2s; 1.625, −11.4 for C 2p; 2.275, −32.4 for O 2s; 2.275, −14.8 for O 2p; 2.300, −11.6 for Tl 6s; 1.600, −5.80 for Tl 6p, 1.900, −9.10 for Fe 4s; 1.900 and −5.32 for Fe 4p. The H_{ii} value for Fe 3d was at −12.60. A linear combination of two Slater-type orbitals with exponents $\zeta_1 = 5.35$ and $\zeta_2 = 1.800$ with the weighting coefficients $c_1 = 0.5366$ and $c_2 = 0.6678$ was used to represent the Fe atomic orbitals. DFT calculations were carried out with the help of the Amsterdam Density Functional (ADF) program [21] developed by Baerends and coworkers [22] using the local density approximation (LDA) in the Vosko–

Table 2
Selected bond lengths (Å) and angles (°) for $[PPN]_3$[**IV**]

Distances			
Tl(1)–Fe(5)	2.553(3)	Tl(1)–Fe(1)	2.609(3)
Tl(1)–Fe(2)	2.664(3)	Tl(1)–Tl(2)	3.5880(13)
Tl(1)–Tl(3)	3.6530(15)	Tl(2)–Fe(3)	2.549(3)
Tl(2)–Fe(2)	2.627(3)	Tl(2)–Fe(1)	2.642(3)
Tl(3)–Fe(4)	2.557(3)	Tl(3)–Fe(2)	2.640(3)
Tl(3)–Fe(1)	2.644(3)		
Angles			
Fe(5)–Tl(1)–Fe(1)	147.40(11)	Fe(5)–Tl(1)–Fe(2)	140.23(10)
Fe(1)–Tl(1)–Fe(2)	72.36(10)	Fe(3)–Tl(2)–Fe(1)	139.50(11)
Fe(3)–Tl(2)–Fe(2)	146.11(11)	Fe(2)–Tl(2)–Fe(1)	72.44(9)
Fe(4)–Tl(3)–Fe(2)	145.47(11)	Fe(4)–Tl(3)–Fe(1)	142.29(11)
Fe(2)–Tl(3)–Fe(1)	72.20(9)	Tl(1)–Fe(1)–Tl(2)	86.20(10)
Tl(1)–e(1)–Tl(3)	88.11(10)	Tl(2)–Fe(1)–Tl(3)	92.35(10)
Tl(2)–Fe(2)–Tl(3)	92.75(9)	Tl(2)–Fe(2)–Tl(1)	85.38(9)
Tl(3)–Fe(2)–Tl(1)	87.05(9)		
C(11)–Fe(1)–C(13)	103.9(11)	C(11)–Fe(1)–C(12)	99.1(12)
C(13)–Fe(1)–C(12)	105.1(10)	C(11)–Fe(1)–Tl(1)	86.3(8)
C(13)–Fe(1)–Tl(1)	164.2(8)	C(12)–Fe(1)–Tl(1)	84.8(8)
C(11)–Fe(1)–Tl(2)	172.3(8)	C(13)–Fe(1)–Tl(2)	83.1(8)
C(12)–Fe(1)–Tl(2)	82.0(8)	C(11)–Fe(1)–Tl(3)	85.6(9)
C(13)–Fe(1)–Tl(3)	80.8(7)	C(12)–Fe(1)–Tl(3)	171.2(9)
C(21)–Fe(2)–C(22)	98.7(11)	C(21)–Fe(2)–C(23)	97.5(11)
C(22)–Fe(2)–C(23)	98.2(9)	C(21)–Fe(2)–Tl(2)	88.9(8)
C(22)–Fe(2)–Tl(2)	82.4(7)	C(23)–Fe(2)–Tl(2)	173.4(8)
C(21)–Fe(2)–Tl(3)	88.6(9)	C(22)–Fe(2)–Tl(3)	171.1(7)
C(23)–Fe(2)–Tl(3)	85.7(6)	C(21)–Fe(2)–Tl(1)	172.6(9)
C(22)–Fe(2)–Tl(1)	85.2(7)	C(23)–Fe(2)–Tl(1)	88.1(8)
C(33)–Fe(3)–C(34)	117.2(12)	C(33)–Fe(3)–C(32)	20.3(11)
C(34)–Fe(3)–C(32)	119.7(12)	C(33)–Fe(3)–C(31)	95.5(10)
C(34)–Fe(3)–C(31)	95.2(11)	C(32)–Fe(3)–C(31)	95.9(10)
C(33)–Fe(3)–Tl(2)	83.4(8)	C(34)–Fe(3)–Tl(2)	80.5(10)
C(32)–Fe(3)–Tl(2)	89.4(7)	C(31)–Fe(3)–Tl(2)	174.4(7)
C(41)–Fe(4)–C(43)	95.7(12)	C(41)–Fe(4)–C(42)	95.7(13)
C(43)–Fe(4)–C(42)	116.1(13)	C(41)–Fe(4)–C(44)	92.5(11)
C(43)–Fe(4)–C(44)	119.5(14)	C(42)–Fe(4)–C(44)	122.5(12)
C(41)–Fe(4)–Tl(3)	177.0(9)	C(43)–Fe(4)–Tl(3)	85.3(9)
C(42)–Fe(4)–Tl(3)	86.4(9)	C(44)–Fe(4)–Tl(3)	84.5(7)
C(51)–Fe(5)–C(54)	94.8(12)	C(51)–Fe(5)–C(52)	93.6(11)
C(54)–Fe(5)–C(52)	123.5(11)	C(51)–Fe(5)–C(53)	97.7(10)
C(54)–Fe(5)–C(53)	118.6(10)	C(52)–Fe(5)–C(53)	115.4(9)
C(51)–Fe(5)–Tl(1)	176.2(8)	C(54)–Fe(5)–Tl(1)	83.6(8)
C(52)–Fe(5)–Tl(1)	84.6(7)	C(53)–Fe(5)–Tl(1)	86.1(6)

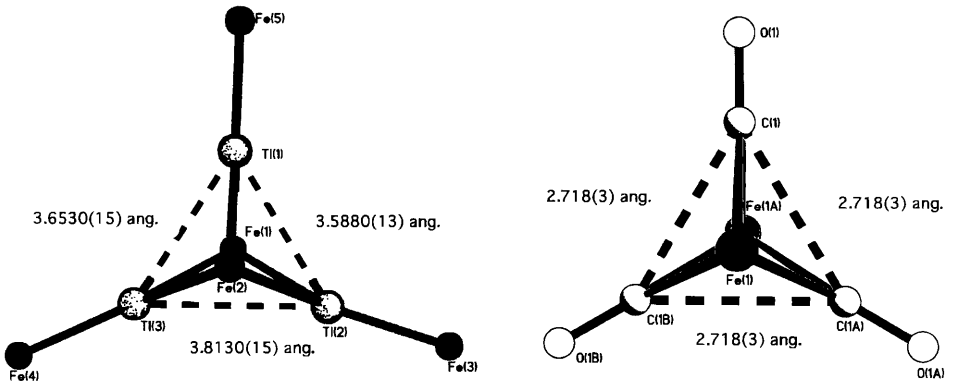

Fig. 2. Comparison of the trigonal planar geometry in $[\mathbf{IV}]^{3-}$ and $Fe_2(CO)_6(\mu\text{-}CO)_3$.

Wilk–Nusair parameterization [23]. The atom electronic configurations were described by a triple-ζ Slater-type orbital (STO) basis set for H 1s, C 2s and 2p, O 2s and 2p and Tl 6s and 6p augmented with a 3d single-ζ polarization for C and O atoms and with a 2p single-ζ polarization for H atom. A triple-ζ STO basis set was used for Fe 3d and 4s augmented with a single-ζ 5p polarization function. A frozen-core approximation was used to treat the core shells up to 1s for C and O, up to 5p for Tl and up to 3p for Fe [22a]. The geometries were fully optimized using the analytical gradient method implemented by Verluis and Ziegler [24].

4. Results and discussion

Three thallium atoms and two iron atoms are arranged in a pseudo trigonal bipyramid in $[PPN]_3[\mathbf{IV}]$. The iron atoms occupy the apical positions with the thallium atoms being found in the equatorial positions. Within the trigonal bipyramid, the Fe–Tl distances range from 2.553(3) to 2.664(3) Å. In addition to the two iron atoms which are part of the cluster core, there are terminal trigonal bipyramidal $Fe(CO)_4$ groups attached to each thallium atom giving these atoms approximately trigonal planar geometry's ($\Sigma_{\text{angles about Tl}} = 357.05–359.99°$). The Fe(1)–Tl–Fe(2) angles (those involving the irons that make up the trigonal bipyramidal core) are acute (72.20(9)–72.44(9)°) while those involving the terminal $Fe(CO)_4$ fragments are almost double those values (140.23(10)–147.44(11)°). The trigonal bipyramidal cage is slightly distorted as the distances between the thallium centers are not equal as shown in Fig. 2. They range from 3.5880(13) to 3.8130(15) Å. There is also a distortion in the position of the terminal $Fe(CO)_4$ group at Fe(3). Whereas Fe(4) and Fe(5) lie less that 0.06 Å out of the Tl(3)–Fe(1)–Fe(2) and the Tl(1)–Fe(1)–Fe(2) planes, respectively, Fe(3) is 0.400 Å away from the Tl(2)–Fe(1)–Fe(2) plane. The equatorial COs of the terminal trigonal bipyramidal $Fe(CO)_4$ groups are tilted slightly toward the Tl atoms as commonly found in main group–element/transition metal complexes of this class.

The related isostructural molecule, $Fe_2(CO)_6\{\mu\text{-}GaSi(SiMe_3)_3\}_3$, [25] has recently been reported. As expected the Fe–Ga bond distances are shorter of than those of Fe–Tl (2.3818(7) versus 2.553(3) Å) since the atomic radius of is Ga approximately 0.18 Å shorter than that of Tl (1.53 versus 1.71 Å) [26]. Additionally, the Ga compound deviates from an ideal trigonal bipyramid in that the Fe–Ga–Fe angles (those involving the irons that make up the trigonal bipyramidal core) are acute (74.28(4)°) while those involving the terminal $SiMe_3$ fragments are almost double those values (142.69(2)°). However, Ga–Ga distances are symmetrical (3.289 (1) Å) similarly to $Fe_2(CO)_6(\mu\text{-}CO)_3$. The Fe–Fe distance is 2.876(1) Å in the Ga compound as compared 3.113(3) Å in the Tl cluster.

An important feature of the $[PPN]_3[\mathbf{IV}]$ molecule compared to the dimeric $[Et_4N]_6[\{\mathbf{IV}\}_2]$ is that the shortest Tl···Tl distance is one tenth of an angstrom shorter than the shortest one in the dimeric form: 3.558(13) and 3.711(1) Å but still a few tenths of an angstrom longer than the Tl–Tl distances in the α form of elemental thallium: 3.4076 and 3.4566 Å [27]. Recently alkali–metal–triel (Tr) systems have shown an abundance of phases containing isolated cluster or network polyanions, especially for Tr = Ga, In and Tl [28]. Among these, typical Tl–Tl distances range from 3.153(3)–3.320(3) Å.

The Tl···Tl distances within a Fe_2Tl_3 unit lie within a much narrower range (3.711(1)–3.773(1) Å) than in the monomeric form. Additionally, the $Fe(CO)_4$ groups which form the bridges between the two monomers are now pseudo octahedral instead of trigonal bipyramidal in order to accommodate coordination by the additional Tl atom.

4.1. Theoretical investigation

In order to analyze and compare the bonding in the $[\{\mathbf{II}\}_2]^{2-}$, $[\{\mathbf{III}\}_2]^{4-}$ and $[\{\mathbf{IV}\}_2]^{6-}$ dimers and their

monomers, a series of EHT and DFT calculations were carried out on various models of the monomeric form as well as on the $[\{\mathbf{II}\}_2]^{2-}$, $[\{\mathbf{III}\}_2]^{4-}$ and $[\{\mathbf{IV}\}_2]^{6-}$ dimers. Looking first at the $[Fe_2(CO)_6\{\mu\text{-}TlFe(CO)_4\}_3]^{3-}$ monomer $[\mathbf{IV}]^{3-}$, one is tempted to describe it with a localized two-electron two-center bonding picture, assuming that the electron deficient Tl atoms are surrounded by only 6 electrons, as is often the case with Group 13 elements. However, this localized picture requires a single bond between the two bridged Fe atoms in order for them to satisfy the 18-electron rule. Owing to the observed Fe···Fe distance (3.12 Å), no bond is expected and one is left with two 17-electron centers, an unsatisfactory description since this compound is clearly diamagnetic. This problem raises the question of the existence of a real Fe–Fe bond in $Fe_2(CO)_6(\mu\text{-}CO)_3$ which has been widely discussed in the literature [2–8]. Although the Fe–Fe separation in $Fe_2(CO)_6(\mu\text{-}CO)_3$ (2.52 Å)[2] is consistent with the existence of a single bond, several theoretical investigations have lead to the conclusion that there is no bond or that the bond is very weak [3–8].

Since $Fe_2(CO)_6(\mu\text{-}CO)_3$ is the first member of the isoelectronic $[Fe_2(CO)_6(\mu\text{-}CO)_{3-n}\{\mu\text{-}TlFe(CO)_4\}_n]^{n-}$ ($n = 0$–3) series, we found it useful to go back first to the description of the main features of its electronic structure, as calculated at the EHT level with the CACAO program [20] which allows a detailed qualitative fragment molecular orbital (FMO) analysis of the rather complicated bonding in this molecule. Then, the three thallium monomers will be compared to the $Fe_2(CO)_6(\mu\text{-}CO)_3$ reference. Our description of the bonding in $Fe_2(CO)_6(\mu\text{-}CO)_3$ is close to that proposed initially by Summerville and Hoffmann [3] and refined

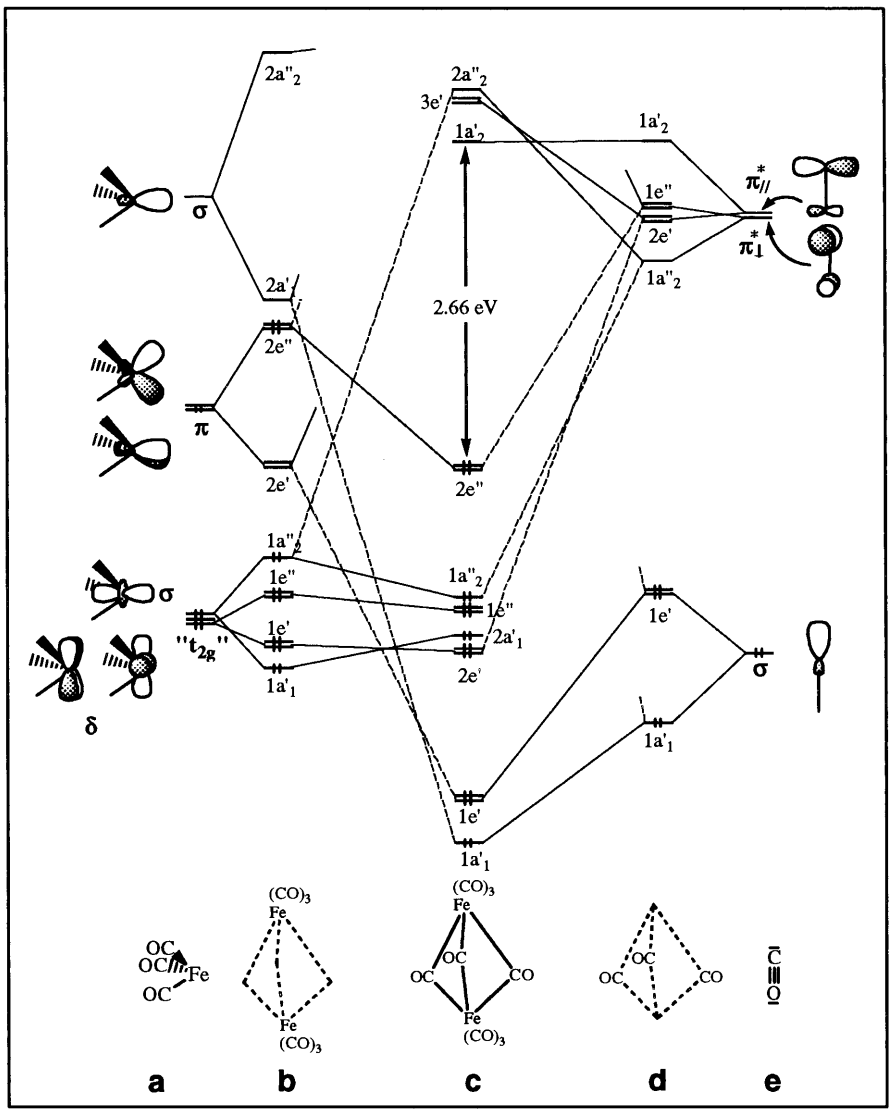

Fig. 3. Qualitative interaction diagram for $Fe_2(CO)_6(\mu - CO)_3$. (a) FMOs of $Fe(CO)_3$. (b) FMOs of the $(CO)_3Fe\cdots Fe(CO)_3$ fragment. (c) MO diagram of $Fe_2(CO)_6(\mu - CO)_3$. (d) FMOs of the $(\mu - CO)_3$ fragment. (e) FMOs of CO.

later by Mealli and Proserpio [5a] and by Rosa and Baerends [6b] The EHT MO interaction diagram of $Fe_2(CO)_6(\mu\text{-}CO)_3$ (D_{3h} symmetry) is sketched in Fig. 3. The molecule can be conceptually divided into two conical $Fe(CO)_3$ fragments and three bridging COs. Each $Fe(CO)_3$ fragment has a set of six FMOs (Fig. 3(a)). The highest in energy is a diffuse σ-type hybrid. It lies above two degenerate π-type hybrids. Being primarily of 3d-type character, the three lowest FMOs are more contracted. One is of σ-type and two are of δ-type. They constitute the so-called t_{2g} set [29]. When the two $Fe(CO)_3$ units are brought together at a separation of 2.52 Å (Fig. 3(b)), each individual $Fe(CO)_3$ FMO gives rise to one bonding and one antibonding combination. Due to their contracted nature, the t_{2g} orbitals overlap more weakly than the hybrid FMOs. As a result, the Fe···Fe overlap population in the σ-bonding $1a_1$ orbital is 0.155, as compared to 0.309 for the $2a_1$ hybrid combination. Clearly, the creation of a strong σ-bond between the metal atoms would require the filling of $2a_1$. When considered as the HOMO of the fragment, the computed total Fe···Fe overlap population is 0.418, while this value is only 0.175 when $1a_1$ is the HOMO.

The σ-type lone pair and π*(CO) orbitals of each individual μ-CO ligand (Fig. 3(e)) combine to give rise to 9 combinations associated with the three bridging ligands (Fig. 3(d)). The occupied $1a_1'$ and $1e'$ lone pair combinations interact preferentially with the vacant $2a_1'$ and $2e'$ hybrid combinations of the dimetallic fragment (Fig. 3(c)). On the other hand, the vacant $1e''$ and $1a_2''$ π*(CO) combinations interact preferentially with the occupied $2e''$and $1a_2''$ levels of the dimetallic fragment. These six two-electron/two-orbital stabilizing interactions can be associated with the making of the six Fe–(μ-CO) bonds. It is noteworthy that, except for $2a_2''$, all the dimetallic hybrid combinations are involved in these bonds. Additional backbonding interaction is obtained by interaction of the $2e'$ π*(CO) level with the occupied $1e'$ t_{2g} combination. In this one-to-one matching of the fragment orbitals, the occupied $1a_1'$ and vacant $2a_2''$ dimetallic levels remain largely unperturbed. If there is a Fe–Fe bond, there should be the bonding and antibonding orbitals associated with it. However, the Fe···Fe overlap population computed for $Fe_2(CO)_6(\mu\text{-}CO)_3$ is repulsive (-0.026). Indeed, the bonding character of the $1a_1'$ level is not large enough to counterbalance the antibonding nature of the occupied e'' and a_2'' levels, and the partial occupation of the $2a_1'$ dimetallic FMO (0.453) does not provide significant additional bonding character. Clearly, due to its contracted nature, the a_1' in-phase MO of $Fe_2(CO)_6(\mu\text{-}CO)_3$ is better described as being an almost non-bonding electron pair delocalized on both metals rather than being a real σ-bonding electron pair. The reason for this weak Fe···Fe repulsion (or perhaps attraction) is that there is competition between metal–metal and metal-(μ-CO) bonding for the use of the $2a_1'$ dimetallic FMO, the winner being metal-(μ-CO) bonding.

When the Fe···Fe separation varies over a reasonable range, the corresponding overlap populations change little. The EHT minimum energy is found for a separation of 2.62 Å. At this distance the Fe···Fe overlap population is low at -0.027 and that for Fe–(μ-CO) is a maximum (0.475).

With one σ-type lone pair and two π-type vacant 6p orbitals, a $\{Tl\text{–}Fe(CO)_4\}^-$ or a Tl–H fragment is isolobal to CO. The substitution in $Fe_2(CO)_6(\mu\text{-}CO)_3$ of the three bridging CO ligands by three Tl–H units gives rise to a very similar interaction diagram for $Fe_2(CO)_6(TlH)_3$ (D_{3h} symmetry), as shown in Fig. 4. At the experimentally-derived intermetallic distance of 3.12 Å, the Fe···Fe overlap population is small, but surprisingly positive (0.064), indicative of a weak through bond interaction. Interestingly, the Tl···Tl overlap population (0.034) is also indicative of some weak through bond attraction. This is due to the diffuse character of the Tl valence orbitals which overlap somewhat at the observed Tl···Tl distances and mix in a bonding way into the occupied levels of the complex. It is interesting to note that, according to the Wade–Mingos rules, [30] two extra electrons occupying a level of a_2'' symmetry would be required for the existence of stronger Tl–Tl bonding [10].

The EHT minimum energy is found for a separation of 3.43 Å. At this distance the Fe–Tl overlap population is close to its maximum (0.252), while the Fe···Fe one (0.028) is still indicative of some weak through-bond interaction. EHT calculations on the real $[Fe_2(CO)_6\{\mu\text{-}TlFe(CO)_4\}_3]^{3-}$ anion gave very similar results. Clearly, the tuning of the intermetallic separation is essentially due to the geometrical constraints of the bridging ligand.

DFT calculations fully confirm the EHT qualitative picture, as shown by the major optimized metrical data computed for the $[Fe_2(CO)_6(\mu\text{-}CO)_{3-n}\{\mu\text{-}TlFe(CO)_4\}_n]^{n-}$ ($n = 0$–3) series which are given in Table 3. There is a good agreement between the theoretical and the available monomer X-ray molecular structures. A similar agreement has been obtained by DFT calculations on $Fe_2(CO)_6(\mu\text{-}CO)_3$ [5c,6b,8] and related Fe/Ga complexes [25]. As expected, the Fe···Fe distance increases significantly with n. The largest variation is found between $n = 2$ and 3. Clearly, bridging CO ligands do not like large Fe···Fe separations. On the other hand, the $(CO)_3Fe\text{–}(\mu\text{-}Tl)$ distance decreases with n whereas the $(CO)_4Fe\text{–}Tl$ distance vary in the other way. All the DFT-computed HOMO-LUMO gaps for the $[Fe_2(CO)_6(\mu\text{-}CO)_{3-n}\{\mu\text{-}TlFe(CO)_4\}_n]^{n-}$ monomers are large (Table 3), in full agreement with their diamagnetic behavior. Optimizations of the isoelectronic $Fe_2(CO)_6(\mu\text{-}CO)_{3-n}(\mu\text{-}TlH)_n$ series gave similar results (not

Table 3
DFT computed HOMO/LUMO gaps and major optimized metrical data (Å) for the $[Fe(CO)_{9-n}\{TlFe(CO)_4\}_n]^{n-}$ ($n = 0$–3) compounds and their dimers [a]

	$Fe_2(CO)_9$	$[Fe_2(CO)_8\{TlFe(CO)_4\}]^{1-}$		$[Fe_2(CO)_7\{TlFe(CO)_4\}_2]^{2-}$		$[Fe_2(CO)_6\{TlFe(CO)_4\}_3]^{3-}$	
Compound symmetry	D_{3h}	Monomer [**II**]$^-$ C_s	Dimer $[\{\mathbf{II}\}_2]^{2-}$ D_{2h}	Monomer [**III**]$^{2-}$ C_s	Dimer $[\{\mathbf{III}\}_2]^{4-}$ C_{2h}	Monomer [**IV**]$^{3-}$ C_{3h}	Dimer $[\{\mathbf{IV}\}_2]^{6-}$ D_{2h}
HOMO/LUMO Gap (eV)	2.98	2.20	2.38	2.11	2.20	2.42	2.02
$(CO)_3Fe\cdots Fe(CO)_3$	2.50 (2.52)	2.60	(2.61)	2.76	2.75 (2.79)	3.11 (3.12)	3.09 (3.09)
$(CO)_4Fe\cdots Fe(CO)_4$			4.25 (4.25)		4.28 (4.25)		4.22 (4.21)
$(CO)_3Fe–Tl_{tricoord}$		2.71		2.69	2.69 (2.65)	2.68 (2.64)	2.67 (2.64)
$(CO)_3Fe–Tl_{tetracoord}$			2.76 (2.75)		2.75 (2.71)		2.77 (2.72)
$(CO)_4Fe–Tl_{tricoord}$		2.53		2.57	2.62 (2.53)	2.61 (2.55)	2.66 (2.56)
$(CO)_4Fe–Tl_{tetracoord}$			2.75 (2.75)		2.79 (2.79)		2.81 (2.80)
Fe–(μ-CO)	1.99 (2.01)	1.97	1.97 (1.99)	1.97	1.97 (1.99)		
$Tl_{tricoor}\cdots Tl_{tricoord}$				3.97		3.79 (3.68)	3.81 (3.72)
$Tl_{tricoord}\cdots Tl_{tetracoord}$					3.97 (3.87)		3.85 (3.77)
$Tl_{tetracoord.}\cdots Tl_{tetracoord}$			3.49 (3.50)		3.60 (3.60)		3.71 (3.70)
$Tl_{tricoord.}\cdots$(μ-CO)		3.32		3.25	3.30 (3.30)		
$Tl_{tetracoord.}\cdots$(μ-CO)			3.33 (3.34)		3.34 (3.24)		
(μ-CO)$\cdots$(μ-CO)	2.68 (2.72)	2.66	2.66 (2.73)				

[a] Averaged experimental values are given in parentheses.

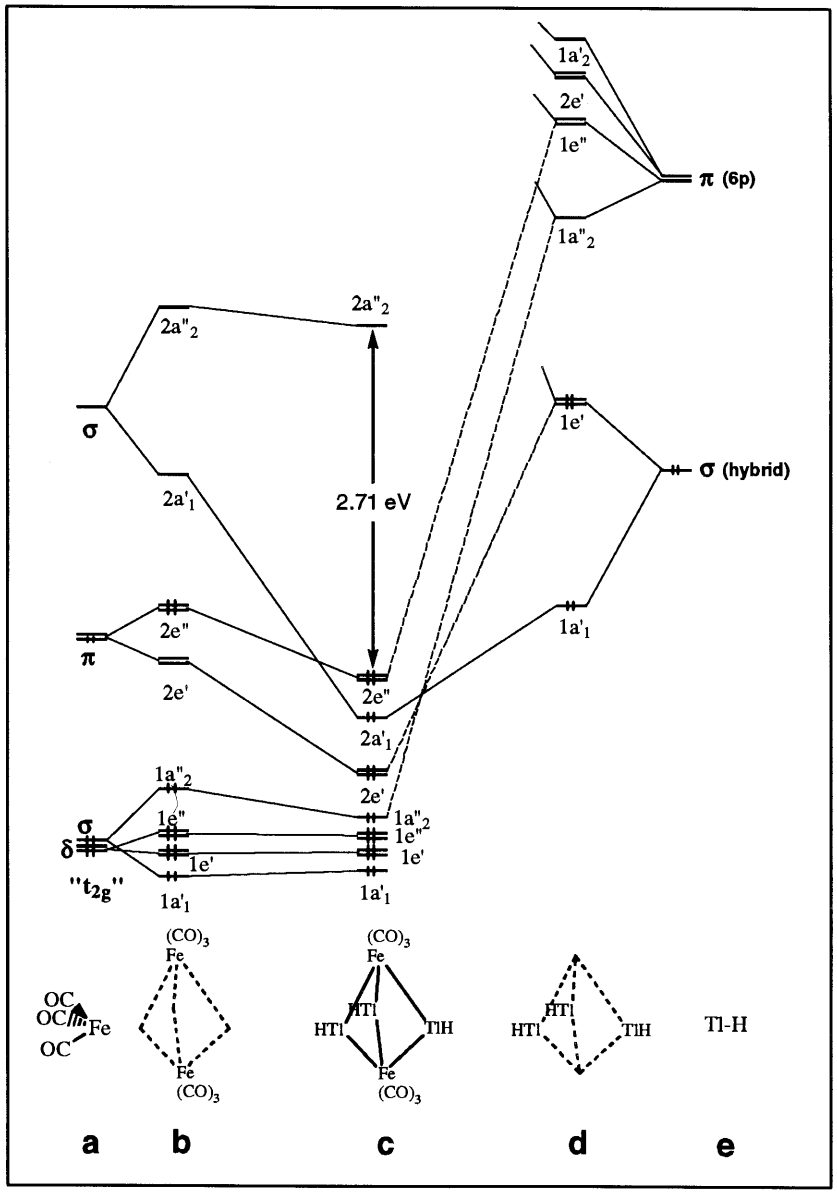

Fig. 4. Qualitative interaction diagram for $\{Fe_2(CO)_6[\mu\text{-}TlH]_3\}^{3-}$. (a) FMOs of $Fe(CO)_3$. (b) FMOs of the $(CO)_3Fe\cdots Fe(CO)_3$ fragment. (c) MO diagram of $\{Fe_2(CO)_6[\mu\text{-}TlH]_3\}^{3-}$. (d) FMOs of the $[\mu\text{-}TlH]_3^{3-}$ fragment. (e) FMOs of $[Tl–H]^-$.

shown here) indicating that the $Fe(CO)_4$ groups play a secondary role in the Fe···Fe and the Fe–(μ-Tl) bonding.

In order to get a more quantitative insight into the variations induced by the substitution of one of several μ-CO ligand(s) by the same number of isolobal TlR units, a DFT fragment analysis was performed which includes an FMO population analysis and decomposition of the fragment bonding energy in the way proposed by Ziegler and coworkers [31] and applied to $Fe_2(CO)_6(\mu\text{-}CO)_3$ by Rosa and Baerends [6b] (Table 4). The Tl model chosen for being compared to $Fe_2(CO)_6(\mu\text{-}CO)_3$ is $Fe_2(CO)_6(TlH)_3$, because it has the same perfect D_{3h} symmetry. Following the analysis of Rosa and Baerends, [6b] the considered $(CO)_3Fe\cdots Fe(CO)_3$ fragment was taken in its $(2e')^0$ $(2e'')^4$ configuration, i.e. prepared for providing the adequate number of two-electron/two-orbital interactions with the three μ-CO ligands (as in Figs. 3 and 4). The energy corresponding to the formation of a $Fe_2(CO)_6(\mu\text{-}X)_3$ (X = CO, TlH) molecule out of the two considered fragments is decomposed into an electrostatic term, a Pauli repulsion term and the different irreducible representation contributions to the orbital interaction energy (Table 3) [31]. The Pauli repulsion term can be interpreted as resulting from the four-electron/two-orbital destabilizing interactions whereas the orbital interaction term results from the two-electron/two-orbital bonding inter-

actions. Our DFT results on $Fe_2(CO)_6(\mu\text{-}CO)_3$ differ somewhat to those of Rosa and Baerends [22c] because of the different choices of basis sets and functionals, but the trends are similar: the strongest bonding interactions are associated to the e′ and e″ orbitals, while the participation to the bonding of the a'_1 and a''_2 FMOs is significantly lower. A somewhat different situation arises in $Fe_2(CO)_6(\mu\text{-}TlH)_3$, where the e′ contribution dominates largely and the a''_2 one is very small. Clearly, because of the different Fe···Fe and Fe–X distances in $Fe_2(CO)_6(\mu\text{-}X)_3$ (X = CO, TlH), the FMOs overlap differently in both compounds. The Mulliken populations of the frontier orbitals of the interacting fragments are given in Table 5. The strongest e′ bonding interaction in the case of X = TlH is consistent with a largest electron transfer from the 1e′ FMO of the bridging ligand fragment into the 2e′ FMO of the dimetallic unit. On the other hand, there is less Fe→X electron transfer associated with the a'_1 and e″ interaction in the Tl compound. In both compounds the populations of the a'_1 and a''_2 FMOs of the $(CO)_3Fe\cdots Fe(CO)_3$ fragment are about the same. The main difference is found in the occupation of the weakly Fe···Fe bonding 2e′ FMO, which provides the Tl species with some very weak metal–metal bonding character, despite the large intermetallic separation (3.08 Å). Indeed the DFT-computed Fe···Fe overlap population in this compound is 0.001, as compared to −0.107 for $Fe_2(CO)_6(\mu\text{-}CO)_3$. The DFT-computed Tl···Tl overlap population is also found to be slightly positive (0.032).

Table 4
Energy decomposition (eV) for the formation of $Fe_2(CO)_6(\mu\text{-}X)_3$ (X = CO, TlH) from its $(CO)_3Fe\cdots Fe(CO)_3$ and $(\mu\text{-}X)_3$ fragments [a]

	$Fe_2(CO)_6(\mu\text{-}X)_3$	
	X = CO	X = TlH
Electrostatic	−12.56	−14.37
Pauli repulsion	15.24	14.36
a'_1	−1.63	−1.87
a'_2	−0.20	−0.04
e′	−6.91	−8.82
a''_1	−0.01	−0.03
a''_2	−1.12	−0.37
e″	−6.92	−2.19
Total (including fit corrections)	−14.03	−13.24

[a] The dimetallic unit is considered in the $(2e')^0(2'')^4$ configuration, see text.

Table 5
Mulliken occupation of the frontier orbitals of the $(CO)_3Fe\cdots Fe(CO)_3$ and $(\mu\text{-}X)_3$ fragments in the $Fe_2(CO)_6(\mu\text{-}X)_3$ (X = CO, TlH) complexes

		$Fe_2(CO)_6(\mu\text{-}X)_3$	
		X = CO	X = TlH
$(CO)_3Fe\cdots Fe(CO)_3$ fragment			
Hybrid combinations	$2a''_2$	0.01	0.00
	$2a'_1$	0.63	0.55
	2e″	2.94	3.16
	2e′	1.38	2.14
t_{2g} combinations	$1a''_2$	1.86	1.95
	1e″	3.90	3.94
	1e′	3.60	3.82
	$1a'_1$	1.96	1.94
$(\mu\text{-}X)_3$ fragment			
π-type combinations	$1\ a'_2$	0.01	0.00
	1e″	1.14	0.86
	2e′	0.36	0.24
	$1a''_2$	0.14	0.15
σ-type lone pair combinations	1e′	2.72	1.90
	$1a'_1$	1.42	1.62

4.2. The Effect of dimerization

We turn now the discussion to the bonding analysis of the $[\{\mathbf{II}\}_2]^{2-}$, $[\{\mathbf{III}\}_2]^{4-}$ and $[\{\mathbf{IV}\}_2]^{6-}$ dimers. The formation of the dimers through the formation of two Tl–$Fe(CO)_4$ bonds can be simply described as resulting from the donation of $Fe(CO)_4$ metal lone pairs to thallium centers. The dimerization reduces the electron deficiency of two Tl atoms, but is not expected to significantly modify the Fe···Fe interaction. The major optimized metrical data computed for the $[\{\mathbf{II}\}_2]^{2-}$, $[\{\mathbf{III}\}_2]^{4-}$ and $[\{\mathbf{IV}\}_2]^{6-}$ dimers are given in Table 3. There is a good agreement between the theoretical and the X-ray molecular structures [9–11]. Except for rehybridation around the bridging $Fe(CO)_4$ groups and around the tetracoordinated Tl atoms, no big difference arises from the comparison of the optimized structures of the dimers with their monomers. A small shortening of the Fe···Fe separation upon dimerization can be noticed. As expected, the thallium atoms which are involved in the bonds between the monomers are less positively charged in the dimers. For example, in $[\mathbf{IV}]^{3-}$ and $[\{\mathbf{IV}\}_2]^{6-}$ the corresponding thallium Mulliken populations are 0.291 and 0.123, respectively. The bonding energy associated with the formation of $[\{\mathbf{II}\}_2]^{2-}$ from two free monomers is computed to be 0.38 eV. This is a reasonable value, owing to the fact that the $[\{\mathbf{II}\}_2]^{2-}$ dimer is observed in solution. From this perspective, lower bonding energies are expected for $[\{\mathbf{III}\}_2]^{4-}$ and $[\{\mathbf{IV}\}_2]^{6-}$. Unfortunately, as often observed with calculations carried out on isolated highly charged anions, the highest occupied levels are found to lie at positive energies, giving rise to unreliable repulsive interaction energies between the monomers. Although overestimated in the calculations, the ionic repulsion between monomers is likely to be significant and is probably one of the factors preventing further oligomerization.

5. Conclusions

Although the metal–metal separation varies from short (2.52 Å, $n = 0$) to very long (3.12 Å, $n = 3$) in the isoelectronic $[Fe_2(CO)_6(\mu\text{-}CO)_{3-n}\{\mu\text{-}TlFe(CO)_4\}_n]^{n-}$ ($n = 0$–3) series, the nature of the Fe···Fe interaction is quite similar within the series. Because only one σ-type frontier orbital on each $Fe(CO)_3$ fragment is capable of significantly overlapping with the other metal and with the bridging ligands, a competition arises that favors bonding with the bridging ligands over the formation of a Fe–Fe single bond. Therefore, the weak (bonding or antibonding) metal–metal interaction results from a balance between various through-bond interactions and repulsion between the metal lone pairs. Our results show clearly that in all these compounds, the Fe···Fe separation is mainly driven by the nature and size of the various bridging ligands. A localized Lewis formula in which a Fe–Fe single bond is drawn appears inappropriate. Rather, two mesomeric formulae in which no Fe–Fe bond is present and exhibiting one 18-electron Fe^{-I} and one 16-electron Fe^{+I} would be more satisfying. This localized picture raises the question of electron deficiency on the metals and suggests the existence of an acceptor orbital delocalized on both metals. This orbital can be identified as deriving from the 2a″ FMO of the $(CO)_3Fe\cdots Fe(CO)_3$ fragment. Due to its hybrid nature, it lies at a rather high energy and therefore the iron centers are not strong acceptors.

Another way of looking at the electronic structure of the $[Fe_2(CO)_6(\mu\text{-}CO)_{3-n}\{\mu\text{-}TlFe(CO)_4\}_n]^{n-}$ ($n = 0$–3) species is to describe them as resulting from the interaction between two metal centers lying in an octahedral environment, both octahedral sharing a triangular face. Each of the $(CO)_3Fe(\mu\text{-}X)_{3/2}$ ($X = CO$, $[TlFe(CO)_4]^-$) units exhibits a set of three t_{2g} non-bonding orbitals (one of σ-type and two of δ-type) occupied by five electrons. The building of a single bond through the interaction between two singly occupied σ-type t_{2g} orbitals is expected. However, they overlap poorly (even in $Fe_2(CO)_6(\mu\text{-}CO)_3$) and both σ in-phase ($2a'_1$) and σ out-of-phase ($1a''_2$) combinations remain non-bonding at low energy, and, surprisingly are both occupied. The question which arises then is: where are the two extra electrons which occupy the t_{2g} $1a''_2$ combination coming from? In fact, they can be considered as being one of the Fe–(μ-CO) bonding electron pairs. In a regular species, this bonding pair should lie in an orbital where the iron participation is primarily of 4s and $4p_z$ character, leaving the $3d_\sigma$ orbitals for metal–metal bonding. In the studied compounds this hybrid-type a''_2 MO is high-lying and vacant. Clearly, this is a level crossing between two orbitals of a″ symmetry which is responsible for the absence of a real bond between the metal atoms.

The dimerization of the $[Fe_2(CO)_6(\mu\text{-}CO)_{3-n}\{\mu\text{-}TlFe(CO)_4\}_n]^{n-}$ ($n = 1$–3) compounds allows the lowering of the electron deficiency of Tl atoms through donation from an iron lone pair, leaving almost unchanged the bonding within the associated monomers. The stability of the dimers with respect to dissociation appears to be limited by the destabilizing ionic interaction between the negatively charged monomers.

6. Supplementary material

Crystallographic Data for the structural analysis have been deposited with the Cambridge Crystallographic Data Center, CCDC no. 148020 for $[PPN]_3[Fe_2(CO)_6\{\mu\text{-}TlFe(CO)_4\}_3]$. Copies of this information may be obtained free of charge from The Director, CCDC, 12 Union Road, Cambridge CB2 1EZ, UK (Fax: +44-1223-336033; e-mail: deposit@ccdc.cam.ac.uk or www:http://www.ccdc.cam.ac.uk).

Acknowledgements

The Robert A. Welch Foundation and the National Science Foundation are gratefully acknowledged for financial support of this work (KHW). We are also grateful for a joint NSF/CNRS grant to support the collaboration between Rice University and the Université de Rennes. Computing facilities were provided by the IDRIS-CNRS computing center of Orsay, France.

References

[1] H.M. Powel, R.V.G Ewens, J. Chem. Soc. (1839) 286.
[2] F.A. Cotton, J.M. Troup, J. Chem. Soc. Dalton Trans. (1974) 800.
[3] (a) J.W. Lauher, M. Elian, R.H. Summerville, R. Hoffmann, J. Am. Chem. Soc. 98 (1976) 3219. (b) R.H. Summerville, R. Hoffmann, J. Am. Chem. Soc. 101 (1979) 3821.
[4] (a) C.W. Bauschlisher, P.S. Bagus, J. Chem. Phys. 81 (1985) 5889. (b) C.W. Bauschlisher Jr., J. Chem. Phys. 84 (1986) 872.
[5] (a) C. Mealli, D. Proserpio, J. Organomet. Chem. 386 (1990) 203. (b) J. Rheingold, E. Hunstock, C. Mealli, New J. Chem. 18 (1994) 465. (c) E. Hunstock, C. Mealli, M.J. Calhorda, J. Reingold, Inorg. Chem. 38 (1999) 5053.
[6] (a) W. Heisjer, E.J. Baerends, Faraday Sym. 14 (1980) 211. (b) A. Rosa, E. Baerends, New J. Chem. 15 (1991) 815.
[7] C. Bo, J.P. Sarasa, J.M. Poblet, J. Phys. Chem. 97 (1993) 6362.
[8] J.H. Jang, J.G. Lee, H. Lee, Y. Xie, H.F. Schaefer III, J. Phys. Chem. (1998) 5298.
[9] K.H. Whitmire, J.M. Cassidy, A.L. Rheingold, R.R. Ryan, Inorg. Chem. 27 (1988) 1347.
[10] K.H. Whitmire, R.R. Ryan, H.J. Wasserman, T.A. Albright, S.K. Kang, J. Am. Chem. Soc. 108 (1986) 6831.
[11] J.M. Cassidy, K.H. Whitmire, Inorg. Chem. 28 (1989) 1432.

[12] K.H. Whitmire, J.C. Hutchison, M.D. Burkart, J. Lee, S. Ezenwa, A.L. McKnight, C.M. Jones, R.E. Bachman, Inorganic Synthesis, vol. 31, Wiley, New York, 1997, p. 220.
[13] W. Hieber, J. Gruber, F.Z. Lux, Anorg. Allg. Chem. 300 (1959) 275.
[14] K.H. Whitmire, J.M. Cassidy, Inorg. Chem. 28 (1989) 1435.
[15] D.F. Shriver, M.A. Drezdon, The Manipulations of Air Sensitive Compounds, Wiley, New York, 1986.
[16] A.J. Gordon, R.A. Ford, The Chemist's Companion, Wiley, New York, 1972.
[17] J.K. Ruff, W.S. Schlientz, Inorg. Synth. 15 (1976) 89.
[18] Sheldrick, G. Bruker AXS, 1997, Madison, WI.
[19] (a) R. Hoffmann, J. Chem. Phys. 39 (1963) 1397. (b) R. Hoffmann, W.N. Lipscomb, J. Chem. Phys. 36 (1962) 2179.
[20] C. Mealli, D. Proserpio, J. Chem. Educ. 67 (1990) 399.
[21] Amsterdam Density Functional (ADF) Program, release 2.0.1, Vrije Universteit, Amsterdam, The Netherlands, 1996.
[22] (a) E.J. Baerends, D.E. Ellis, P. Ros, J. Chem. Phys. 2 (1973) 41. (b) E.J. Baerends, P. Rosa, Int. J. Quantum. Chem. S12 (1978) 169. (c) P.M. Boerrigter, G. te Velde, E.J. Baerends, Int. J. Quantum Chem. 33 (1988) 87. (d) G. te Velde, E.J. Baerends, J. Comput. Phys. 99 (1992) 84.
[23] S.D. Vosko, L. Wilk, M. Nusair, Can. J. Chem. 58 (1990) 1200.
[24] L. Verluis, T. Ziegler, J. Chem. Phys. 322 (1988) 88.
[25] W. Kostler, G. Linti, Chem. Eur. J. 4 (1998) 942.
[26] A.F. Wells, Structural Inorganic Chemistry, Oxford Press, Oxford, 1984, p. 1382.
[27] R.C. Weast, Handbook of Chemistry and Physics, CRC Press, Boca Raton, FL, 1981.
[28] (a) Z.C. Dong, R.W. Henning, J.D. Corbett, Inorg. Chem. 36 (1997) 3559. (b) D.Huang, J.D. Corbett, Inorg. Chem. 38 (1999) 316. (c) S. Uma, J.D. Corbett, Inorg. Chem. 38 3831. (d) R.W. Henning, J.D. Corbett, Inorg. Chem. 38 3883.
[29] T.A. Albright, J.K. Burdett, M.H. Whangbo, Orbital Interactions in Chemistry, Wiley, New York, 1985.
[30] (a) K. Wade, in: B.F.G. Johnson (Ed.), Transition Metal Clusters, Wiley, Chichester, UK, 1982, 193. (b) D.M.P. Mingos, D.J. Wales, Introduction to Cluster Chemistry, Prentice Hall, Engelwood Cliffs: New Jersey, 1990.
[31] (a) T. Ziegler, A. Rauk, Theoret. Chim. Acta. 46 (1977) 1. (b) T. Ziegler, J. Am. Chem. Soc. 105 (1983) 7543. (c) T. Ziegler, V. Tschinke, A. Becke, Polyhedron 6 (1987) 685.